The sensitivity of future ocean oxygen to changes in ocean circulation

Jaime B. Palter^{1*}, David S. Trossman^{2,3}

*

- ¹Graduate School of Oceanography, University of Rhode Island, Narragansett, RI,USA
- ²Goddard Earth Sciences Technology and Research, Greenbelt, Maryland
- Department of Earth and Planetary Sciences, The Johns Hopkins University, Baltimore, Maryland
- *Both authors contributed equally to this work.

Key Points:

- The pace and pattern of ocean deoxygenation is largely determined by subgridscale mixing
- De-oxygenation is also influenced by changes in ocean circulation, especially in the

 Southern Ocean and Pacific OMZ
 - Unique modeling framework reveals that ocean circulation perturbations may slow deoxygenation on decadal scale, despite AMOC slowdown

Corresponding author: Jaime B. Palter, jpalter@uri.edu

Abstract

16

17

18

19

20

21

22

23

24

26

27

28

29

30

31

32

37

38

39

40

41

43

45

46

47

A decline in global ocean oxygen concentrations has been observed over the 20th century and is predicted to continue under future climate change. Here, we use a unique modeling framework to understand how the perturbed ocean circulation influences the rate of ocean deoxygenation in response to a doubling of atmospheric CO₂ and associated global warming. In one ensemble of simulations, we artificially hold ocean circulation steady by substituting preindustrial velocity fields while the rest of the climate responds freely to the doubling of atmospheric CO2; in a second ensemble, the ocean circulation responds freely to the climate perturbation. In both simulation types, oxygen declines under warming and these declines have similar spatial patterns. Thus, we first conclude that changes in ocean mixing and O₂ solubility, rather than perturbations to the large-scale circulation, are responsible for the first-order response of ocean oxygen to warming. However, in our simulations, the ocean circulation response to CO₂ doubling slows the pace of future oxygen loss by an average of 20%. This stabilizing effect on oxygen primarily arises from the sensitivity of dense water formation in the Southern Ocean to the perturbed circulation in the model, and, to a lesser extent, from the reduction of export productivity and associated respiration in the ocean interior. A slowdown of the Atlantic Meridional Overturning Circulation increases the residence time of the deep Atlantic Ocean, but on the decadal time scale analyzed here, this aging of the water column does not result in a major oxygen decline, because respiration is slow at these depths. The simulations show that the decrease in O2 solubility associated with ocean warming is slightly greater than the actual realized decrease in preformed O₂ concentrations, particularly at high latitudes, where circulation changes reduce the proportion of undersaturated waters sinking into the ocean interior. Finally, in the tropical Pacific oxygen minimum zone, we show that a predicted weakening of the Walker Circulation would slow the regional upwelling of nutrients and the associated export productivity and respiration, thereby preventing the intensification of low oxygen concentrations there.

1 Introduction

Large-scale oceanic oxygen loss has been observed over the last century [*Ito et al.*, 2017; *Schmidtko et al.*, 2017] and is predicted to continue in response to anthropogenic climate change [*Sarmiento et al.*, 1998; *Bopp et al.*, 2002]. Such oxygen loss can alter ocean ecosystem structure [*Deutsch et al.*, 2015] and fisheries [*Stramma et al.*, 2011]. Another important consequence is the expansion of the ocean's anoxic regions where microbes remove

bioavailable nitrogen from the world's oceans during anaerobic respiration [Stramma et al., 2008; Cabré et al., 2015]. A fraction of oceanic deoxygenation under anthropogenic warming is due to simple thermodynamics, since the solubility of oxygen in seawater is diminished with increasing temperature. However, much of the observed and projected ocean oxygen loss is instead due to shifting ocean dynamics in the context of a changing climate [Ito et al., 2017; Schmidtko et al., 2017; Bopp et al., 2002]. Indeed, climate models predict a number of changes to the ocean that are likely to influence future oceanic oxygen concentrations in addition to the solubility decline: Changes in the biological pump, wind-driven circulation, and the convective renewal of deep water and the associated overturning circulation may all influence ocean oxygen in a warmer world [Matear and Hirst, 2003; Deutsch et al., 2014; Cabré et al., 2015].

49

50

51

52

53

54

55

58

60

61

62

63

64

65

66

67

70

71

72

73

74

75

76

77

79

The evolution of the oxygen budget is typically thought to be governed by the sum of changes in biological consumption of O2 in the ocean interior versus changing concentrations in a well-oxygenated surface mixed layer: $\Delta O_2 = \Delta O_2^{pref} - \Delta O_2^{remin}$. Here, O_2^{pref} is the oxygen concentration at the ocean's surface, which is primarily a function of temperature, and O_2^{remin} is the remineralized oxygen, i.e. the O_2 consumed by respiration in the ocean interior. Various modeling studies have used this decomposition to suggest that only about a quarter of ocean deoxygenation is due to changes in surface concentrations linked to warming temperatures [Bopp et al., 2002; Sarmiento et al., 1998]. Most of the remaining oxygen loss is tied to shifting dynamics that increase O_2^{remin} by slowing down the processes that transport oxygen into the ocean interior. However, we presently lack understanding of how shifting large-scale circulation, such as a slowdown in the Atlantic Meridional Overturning Circulation (AMOC), versus changes in isopycnal and diapycnal mixing, control ocean oxygen concentrations [Schmidtko et al., 2017]. Moreover, there is currently no consensus about the future development of the volume of hypoxic and suboxic waters in the open ocean, due in part to uncertainties in the future of tropical ocean dynamics [Ciais et al., 2013; Cabré et al., 2015].

Here, we approach this challenge with a unique modeling tool. We run two 3-member ensembles of coupled climate model simulations, in which atmospheric CO_2 increases at 1% per year until doubling. In one ensemble, the entire climate system responds to the resulting warming as is standard for a climate sensitivity study. In a second ensemble, the ocean velocities are replaced with the velocities from a control simulation with constant CO_2 , an idealization used by *Winton et al.* [2013] and *Trossman et al.* [2016] to reveal which aspects

of the climate system are sensitive to ocean circulation changes. A comparison of the results between the simulations allows us to separate the circulation-driven changes in O_2 concentrations from all other causes. In addition, a comparison of O_2^{pref} and O_2^{remin} in the two simulation types untangles the distinct role of a perturbed ocean circulation on solubility-driven and respiration-driven oxygen changes.

Our exploration is organized as follows. In the next section we describe the model simulations and metrics used to assess the mechanisms involved in changing oceanic O_2 concentrations. In section 3.1 we examine the globally-averaged response of the ocean oxygen reservoir to the doubling of CO_2 , with and without the ocean circulation response. Further, we consider the degree to which this response is due to the thermally-driven O_2 loss linked to changing surface heat fluxes, the change in the biological pump, and the large scale circulation changes. The roles of isopycnal and diapycnal mixing are inferred, but not explicitly diagnosed, from the residual of an oxygen budget in the two simulation types. Here, we also use maps and meridional sections to look at the spatial patterns of changes in the oxygen reservoir. The results of this spatial analysis leads to a focus on the Pacific Oxygen Minimum Zone (OMZ; Section 3.2), which is an area of acute interest due to both its status as the largest region of pelagic anoxia in the global ocean [Bianchi et al., 2012], and because its response to warming is strongly mediated by the projected perturbation to coupled ocean-atmosphere dynamics. Finally, we conclude and offer an outlook for the future in Section 4.

2 Methods

All simulations were run using the Geophysical Fluid Dynamics Laboratory (GFDL) Climate Model version 2 (CM2.1) at coarse resolution (CM2Mc). CM2Mc uses the same physical oceanic, atmospheric, and sea ice code as the Earth System Model with the Modular Ocean Model (ESM2.1; [Dunne et al., 2012]), with minor alterations as required to adjust to the coarser discretization [Galbraith et al., 2011]. The ocean component is the Modular Ocean Model (MOM5) at nominal 3° resolution. MOM5 uses a tripolar grid with enhanced latitudinal resolution near the equator and at midlatitudes, benefiting the resolution of equatorial currents. There are 28 vertical levels unevenly distributed with a finer resolution toward the surface. Eddy mixing is represented using the parameterization of Gent and McWilliams [1990] with a spatially varying diffusion coefficient [Griffies et al., 2005]. This parameterization has been shown to be effective at qualitatively representing the net effect of mesoscale eddies on property transport in the ocean and its evolution due to warming,

though with some quantitative differences from simulations that resolve eddies. Therefore, the use of a model with parameterized eddies implies one source of uncertainty in our analysis [Griffies et al., 2015; Bryan et al., 2014]. The atmosphere employs the M30 grid, with a nominal latitudinal (longitudinal) resolution of 3 (3.75) degrees and 24 vertical levels. The CM2Mc land component is the Land Dynamics model of Milly and Shmakin [2002], which includes a river routing scheme but no terrestrial ecosystem.

Galbraith et al., [2011] evaluated the CM2Mc control simulation with a focus on radiocarbon, an excellent tracer of ocean ventilation. Their paper showed that both surface radiocarbon distributions and meridional sections through the Atlantic and Pacific are qualitatively very similar to modern, natural (i.e. bomb-corrected) radiocarbon observations, suggesting that the model faithfully simulates the large-scale pathways of ocean ventilation and is an appropriate tool for this study.

Ocean biogeochemistry is solved with the Biogeochemistry with Light, Iron, Nutrients and Gases (BLING) model [Galbraith et al., 2015], an intermediate complexity biogeochemistry model constructed around a core of only six prognostic tracers. BLING includes parameterized, implicit representations of macronutrient, iron, and light limitation and photoadaptation. A recent comparison of BLING against GFDL's full-complexity biogeochemical model, TOPAZ, shows that this model captures many of the most important processes governing the evolution of macronutrients and oxygen, including the response of ocean oxygen to a doubling of atmospheric CO₂ [Galbraith et al., 2015]. Thus, this model provides an adequate tool with which to explore the role of ocean circulation on oxygen at a reduced computational cost, which is amenable to our ensemble approach (3 simulations for each model type) and is helpful for running an idealized configuration of the ocean model that requires a shortened time step.

Our simulations include a control run, in which atmospheric CO_2 concentrations are held steady at 270 ppm. We then ran an idealized climate change simulation in which atmospheric CO_2 increases at 1% per year until doubling during year 70. Next, we ran a second climate change simulation, in which we replace the ocean velocity field with that from the control simulation [*Trossman et al.*, 2016]. This simulation is called V_{fixed} , to signify that the ocean velocities are fixed to their monthly mean preindustrial control values (compared with V_{free} , the more standard model integration, in which all components of the ocean and climate system freely vary). Because the drift in a simulation with velocities held fixed might

be different from the normal (V_{free}) control simulation, we also run a 3-member ensemble of the V_{fixed} control simulation (i.e. with atmospheric CO₂ held at 270 ppm and ocean velocities replaced with those from the V_{free} control simulation). This creates a total of 12 simulations: 3 ensemble members x 2 model configurations (V_{free}) and V_{fixed} x 2 CO₂ boundary conditions (constant and doubling). All effects of climate change are presented after removing drift, by differencing each variable's appropriate control simulation from the climate change simulations (e.g. the drift in the control simulation from V_{fixed} is subtracted from the CO₂ doubling scenario in V_{fixed}). In practice, the drift in both simulation types was small, an advantage of using the monthly-varying ocean currents from the V_{free} control simulation instead of a fixed monthly climatology, as had been done in a previous study [Winton et al., 2013].

The O_2 budget is usefully decomposed into a preformed component (O_2^{pref}) and the component removed by respiration, $O_2^{remin} = O_2^{pref} - O_2$, where O_2 is the *in situ* O_2 concentration in the water column. BLING includes an O_2^{pref} tracer that tags all O_2 at the ocean surface and then tracks this preformed concentration as a passive, conservative tracer, which allows the calculation of the O_2^{remin} in the ocean interior. It is more common to estimate oxygen consumption from the Apparent Oxygen Utilization, $AOU = O_2^{sat} - O_2$, where O_2^{sat} is the oxygen saturation, which can be calculated from temperature and salinity alone. A known weakness with assuming that AOU accurately approximates O_2^{remin} is that water masses may enter the ocean interior without having come into equilibrium with the atmosphere [Ito et al., 2004; Duteil et al., 2013]. This error generally leads to an overestimation of respiration in the ocean interior, since the dense water masses that fill a large volume of the ocean interior are typically understaturated at the end of formation, owing to the low oxygen concentrations of their source waters and relatively brief time for equilibration with the atmosphere. Our use of the explicit O_2^{pref} tag in BLING avoids the assumption of oxygen saturation in the surface waters, thereby eliminating this bias. In Section 3.1, we evaluate how our interpretation of the mechanisms causing ocean deoxygenation would have changed if we had used AOU as a proxy for O_2^{remin} .

3 Results and Discussion

145

146

147

148

149

150

151

152

155

163

164

165

166

167

168

173

174

175

176

177

178

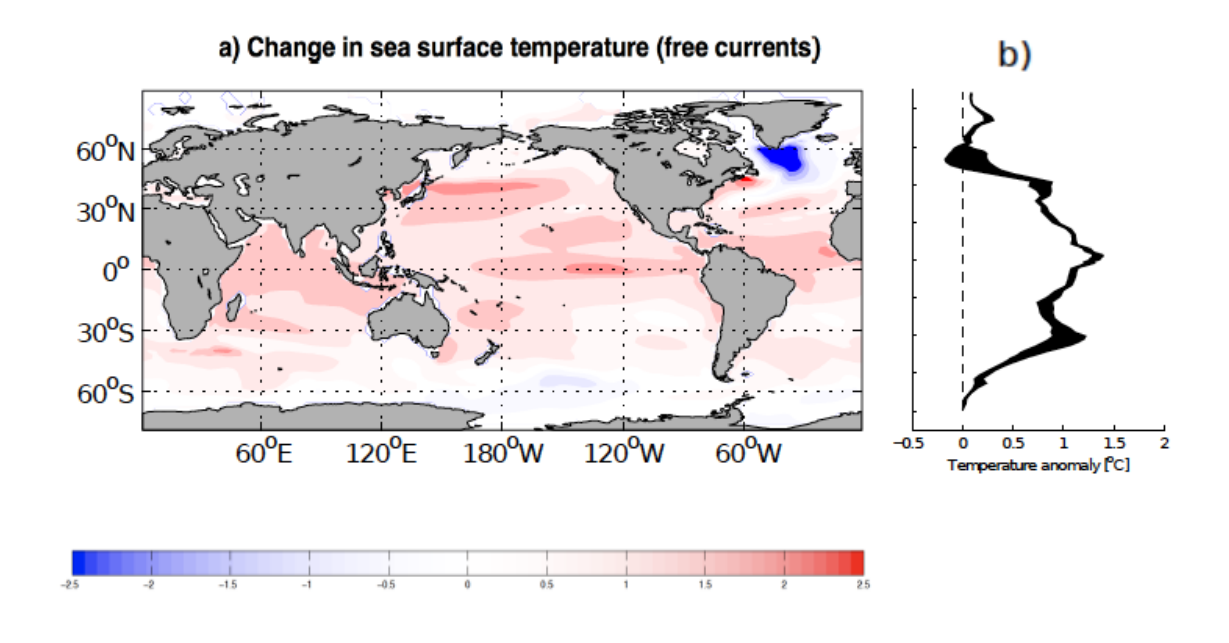
179

180

182

Before discussing the differences in the oxygen change under a doubling of CO_2 under free and fixed ocean circulation regimes, it is important to point out the notable climate differences between these simulations. By the time atmospheric CO_2 doubles in year 70, the

Atlantic Meridional Overturning Circulation (AMOC), defined as the maximum Atlantic zonal mean northward transport at 42°N, has slowed by 25% in V_{free} . Similarly, the deeper



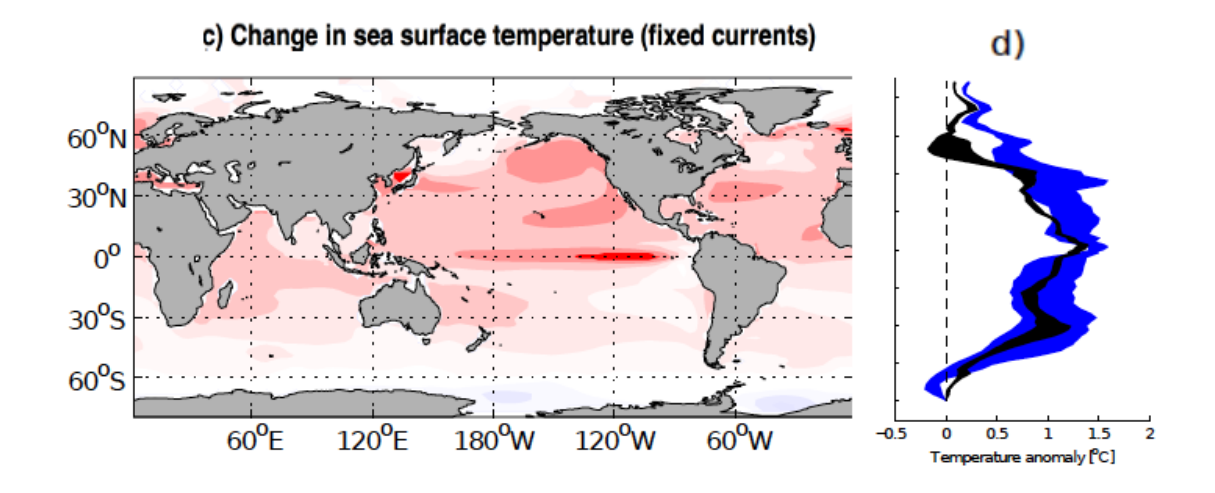


Figure 1. The change in sea surface temperature under a doubling of CO_2 . In this figure, as in all that follow, the change is calculated as the difference between CO_2 doubling simulation and the appropriate control simulation, both averaged over years 61-80 (CO_2 doubles by year 70 and is held constant at 540 ppm thereafter). Panels a-b show the V_{free} simulation; and c-d the V_{fixed} simulation. Panels b and d show the zonal mean of the maps to their left. In panel d, the zonal mean sea surface temperature change from the V_{free} simulation (black) is reproduced for comparison.

156

157

158

159

160

161

overturning circulation that transports Antarctic Bottom Water northward from the Southern Ocean has slowed by 14%. These changes are suppressed in V_{fixed} [Trossman et al., 2016]. Feedbacks between the ocean circulation perturbation and radiative properties of clouds and sea ice lead to a cooler planet relative to the simulation with fixed ocean circulation, particularly in the Northern Hemisphere [Trossman et al., 2016]. Therefore, the global average surface air temperature in V_{free} is 0.4°C cooler than in V_{fixed} , averaged across the three ensemble members of each simulation. Likewise, sea surface temperature (SST) and vertically averaged ocean temperatures are cooler in V_{free} . This stabilizing influence of the AMOC slowdown on planetary temperature is a common feature of climate models [Rugenstein et al., 2012, 2016; Rose et al., 2013; Winton, 2003]. The differences in the spatial pattern of the SST change between V_{free} and V_{fixed} simulations are driven by the slowdown in meridional heat transport in the AMOC and associated cloud and sea ice radiative feedbacks in the mid-to-high latitudes of the Northern Hemisphere: the zonal mean SST north of 40°N is about 2°C cooler in V_{free} than V_{fixed} (Figure 1). These differences affect oxygen solubility, with the lower temperatures of V_{free} maintaining higher solubility, as will be explored below.

3.1 Global Integrals

185

186

187

188

189

190

191

192

195

196

197

198

199

200

202

203

206

207

208

209

210

211

212

213

214

To understand O_2 changes in response to a changing climate, we start from the O_2 conservation equation as in *Bopp et al.* [2002], here shown after eliminating lateral transport by integrating globally:

$$\frac{\partial O_2}{\partial t} = -w \frac{\partial O_2}{\partial z} + \frac{\partial \kappa_v \partial O_2}{\partial z^2} + J_{bio} + J_{flux}$$
 (1)

Here w is the vertical velocity; κ_v is the diapycnal diffusivity; J_{bio} is the biological source minus sink term due to the difference between the biological production of O_2 through photosynthesis and its consumption due to respiration; and J_{flux} is the surface air-sea exchange of O_2 . Table 1 gives the changes in our two ensembles after vertically integrating, where the values are determined by comparing the change over the entirety of the CO_2 doubling simulations after removing any drift in the appropriate constant- CO_2 simulation.

Integrated globally and averaged across the three ensemble members, the V_{free} simulation loses 52 Tmol O₂ year⁻¹ under a doubling of CO₂, which is 20% less than the V_{fixed} simulation loss of 68 Tmol O₂ year⁻¹ (Table 1). Thus, the overall effect of the ocean circu-

lation perturbation is to slow the pace of oceanic deoxygenation. As noted above, the V_{free} simulation is cooler than V_{fixed} upon doubling of CO_2 due to the stabilizing feedbacks associated with the ocean circulation perturbation. These cooler ocean temperatures are expected to provide part of the stabilizing effect on oceanic O_2 concentrations by maintaining higher solubility. However, O_2^{pref} declines approximately equally in both simulations, requiring a closer look.

Bopp et al. [2002] proposed a method to approximate the portion of J_{flux} due to the effect of warming on O_2 solubility, using the net heat flux across the ocean's surface, Q, and the temperature dependence of O_2 solubility:

$$F_{therm} = -\frac{Q}{c_p} \frac{\partial \mathcal{O}_2}{\partial T} \tag{2}$$

where c_p is the heat capacity of water, and T is the sea surface temperature. Because $\frac{\partial O_2}{\partial T}$ is nonlinear, F_{therm} is calculated in every grid box from the monthly heat fluxes from each simulation. This formulation implicitly assumes that the surface ocean is fully saturated in O_2 before any warming begins, and, thus, warming directly translates to an O_2 efflux from the ocean to the atmosphere. However, F_{therm} is 8-11% larger than ΔO_2^{pref} in all three ensemble members of the V_{free} simulation (with the difference even greater in V_{fixed}), implying that the full loss of O_2 due to the solubility decline is not entirely realized. The ΔO_2^{pref} change accounts for about one fifth of the total O_2 loss, slightly lower than one fourth ratio found in a previous study with various models using the F_{therm} diagnostic [Bopp et al., 2002].

As expected, F_{therm} implies a smaller O_2 loss in the cooler simulation; i.e., F_{therm} in V_{free} accounts for that ensemble of simulations losing an average of 12 Tmol year⁻¹ compared to 18 Tmol year⁻¹ for the V_{fixed} simulations (Table 1). Likewise, the saturation oxygen concentration, O_2^{sat} , declines by 30% less in V_{free} than V_{fixed} (Figure 2). Therefore, it is, at first, puzzling that the globally-averaged preformed oxygen concentration, ΔO_2^{pref} , is indistinguishable between the two simulation types. This difference between the saturation and preformed oxygen concentration change is primarily due to the Southern Ocean (Figure 2). Here, in the control simulations, as in nature [Duteil et al., 2013], the oxygen saturation concentration is substantially higher than the actual preformed oxygen concentrations because intermediate and bottom waters sink into the ocean interior before achieving saturation [Duteil et al., 2013]. Under a doubling of CO_2 , the Southern Ocean surface waters

warm approximately 0.5° C in both V_{free} and V_{fixed} (Figure 1). This warming translates in a straightforward way to a decline in O_2^{sat} in both simulation types (Figure 2). However, O_2^{pref} remains constant in the Southern Ocean in V_{free} . The stability of O_2^{pref} in V_{free} in the Southern Ocean – despite ocean warming – suggests that a slowdown in the Southern Ocean overturning reduces the mixing and/or upwelling of O_2 -depleted waters and the associated subduction of undersaturated water masses, i.e. water masses in which $O_2^{pref} < O_2^{sat}$. This effect is exaggerated in V_{fixed} , where the increased water column stability reduces the upward mixing of undersaturated waters and allows the surface to come closer to O_2 equilibrium. The resulting higher O_2^{pref} concentrations are then vigorously subducted into the ocean interior with the pre-industrial circulation fields from the control simulation. In sum, our results emphasize that the simple decomposition $\Delta O_2 = \Delta O_2^{sat} - \Delta AOU$ and the calculation of F_{therm} as in Equation 2 can lead to misleading conclusions about the cause of ocean deoxygenation, particularly in high latitudes.

Table 1. The ensemble mean (min, max) O_2 loss due to various changes under a doubling of CO_2 . Changes are given in Tmol year⁻¹, averaged over the 70 years until CO_2 doubling after removing drift in the appropriate control simulation.

	V_{free} (Tmol year ⁻¹)	V_{fixed} (Tmol year ⁻¹)
Total O ₂ loss	-52 (-60, -44)	-65 (-75, -59)
$\Delta {\sf O}_2^{pref}$	-11 (-13, -8)	-11 (-17, -4)
$\Delta { m O}_2^{remin}$	-41 (-47, -36)	-55 (-58, -54)
Air-sea flux (J_{flux} , Equation 1)	-54 (-61.6, -46)	-64 (-74, -59)
Thermal effect (F_{therm} , Equation 2)	-12 (-14, -9)	-18 (-25, -10)
Biological Pump (J_{bio} , $Equation1$)	2 (1.6, 2)	-0.4 (-0.8, 0)

Since the global, depth-averaged ΔO_2^{pref} is indistinguishable between the two simulation types, the slower deoxygenation in V_{free} versus V_{fixed} is necessarily caused by a slower rate of increase in ΔO_2^{remin} . The globally averaged O_2^{remin} is set by the product of the oxygen utilization rate (OUR) and the average residence time of water in the ocean interior, τ :

$$O_2^{remin} = OUR * \tau \tag{3}$$

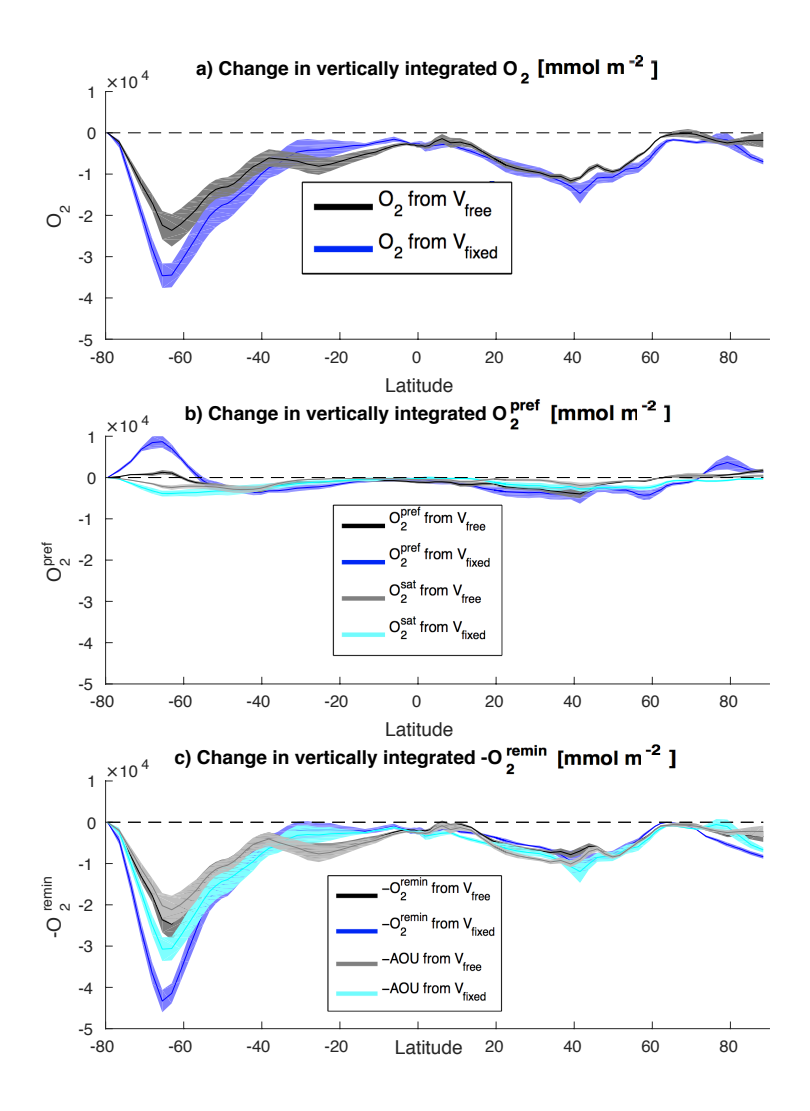


Figure 2. The change in zonally-averaged, vertically-integrated oxygen concentration (mmol m⁻²) under a doubling of atmospheric CO₂ for the (black) V_{free} simulation and (dark blue) V_{fixed} simulation, plotted as a function of latitude. a) Total oxygen concentration. b) O_2^{pref} in black and blue (and and O_2^{sat} in gray and cyan) for V_{free} and V_{fixed} , respectively. c) O_2^{remin} in black and blue (and and AOU in gray and cyan) for V_{free} and V_{fixed} , respectively.

To the degree that the net oxygen utilization rate and residence times are independent, the change in each of these parameters in response to warming reveals the leading cause of the deoxygenation. In our simulations, globally averaged photosynthetic productivity slows under a doubling of CO₂, a common response in Earth System Models to a reduction in the

vertical supply of nutrients under increasing thermal stratification [Cabré et al., 2014]. The slowdown in productivity weakens the export of organic matter from the surface ocean and reduces the substrate fueling respiration in the ocean interior, which is often referred to as a slowdown in the biological pump (Table 1). The climate-driven slowdown in the biological pump prevents the ocean from losing 2 Tmol O_2 year⁻¹ in V_{free} . In V_{fixed} , the use of preindustrial circulation fields, including vertical velocities, largely stabilizes the biological pump and eliminates the associated decrease in O_2 consumption (Figure 3). Thus, the change in the biological pump helps to slow the loss of O_2 when ocean circulation responds to global warming, and explains about 15% of the difference in the O_2 loss between V_{free} and V_{fixed} .

It is clear, however, that the reduction in export productivity in V_{free} does not correspond to an overall reduction in O_2^{remin} . Quite the contrary, it has become well known that a reduction in respiration rates tied to declining export productivity is easily overwhelmed by a slowdown in oxygen renewal via transport and mixing of oxygen into the ocean interior [Gnanadesikan and Marinov, 2008; Bernardello et al., 2014]. In other words, though the rate of respiration declines, the rate of ventilation declines faster. Thus, Table 1 shows that the O_2^{remin} increase for the global ocean is due entirely to an increase in the ocean residence time, and in spite of decreased respiration rates. In our model, this residence time is recorded with an ideal age tracer, which is a tag that is set to zero in the surface layer and ages at one day per day in the ocean interior. On average, the ocean ideal age increases by 6 years in V_{free} and 9 years in V_{fixed} under a doubling of CO_2 .

The increase in ideal age in both simulations is caused by a decline in exchange between the surface and interior ocean, as is common in ocean models experiencing increased vertical buoyancy stratification in a warming climate [Sarmiento et al., 2004]. It is surprising that the ocean circulation perturbation slows the globally averaged aging of the ocean relative to the simulation with fixed circulation. Figure 4 suggests that one cause of the slower aging in V_{free} relative to V_{fixed} is the maintenance of its deep mixed layers along the Antarctic shelf in the Ross Sea. The relative maintenance of mixed layers south of 50°S slows the aging of the water column and associated net decline of oxygen due respiration exceeding O_2 supply (i.e. ΔO_2^{remin}) (Figure 5). We acknowledge that the representation of mixed layer processes on the shelf is parameterized and lacks some key processes, such as interaction with ice shelf cavities. Therefore, although ocean circulation is known to play a key role in upper ocean heat budgets [e.g. Kelly, 2004; O'Reilly et al., 2016] and is accordingly implicated in the evolution of the ocean mixed layer, it is not clear that our result showing that the

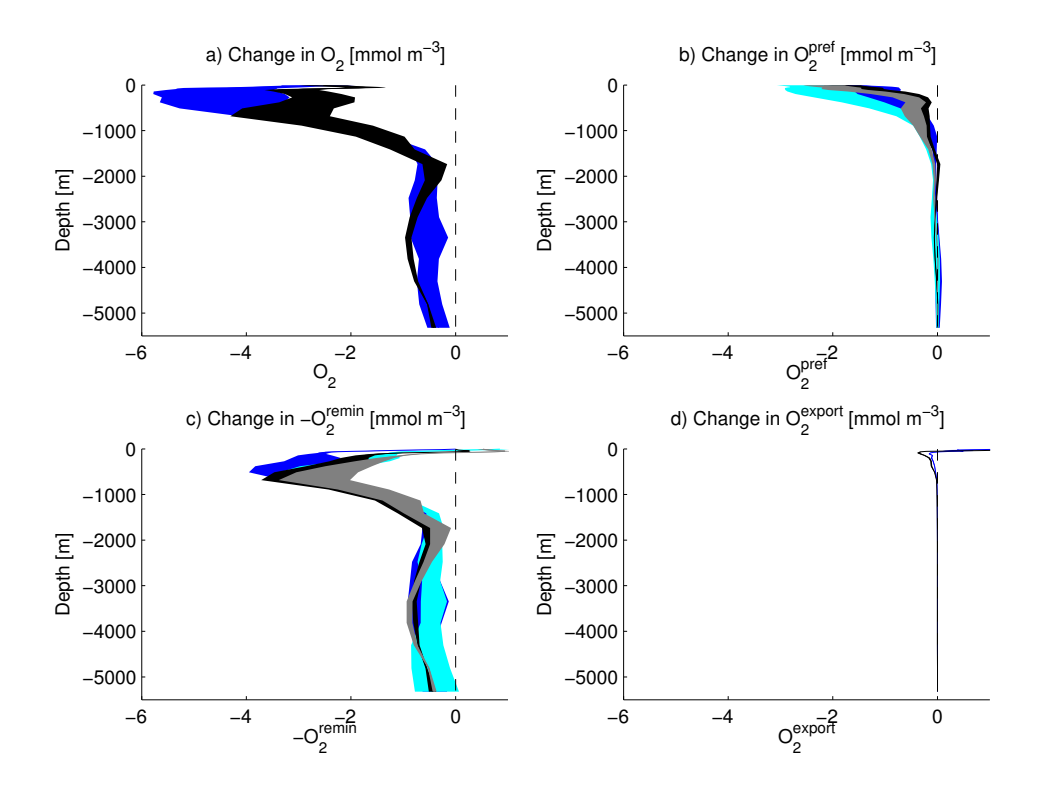


Figure 3. Vertical profiles of the change in globally averaged oxygen concentration (mmol m⁻³) in the ensemble mean of (black) V_{free} and (dark blue) V_{fixed} . a) Total oxygen concentration change. b) O_2^{pref} (and O_2^{sat} in gray and cyan, as in Figure 2). c) O_2^{remin} (and and -AOU in gray and cyan). Here O_2^{remin} and AOU are multiplied by negative one to reflect that an increase in O_2^{remin} corresponds with a decrease in oceanic oxygen concentrations. d) Change in the oxygen utilization rate, OUR, due to change in export productivity, calculated as $O_2^{export} = -150 \frac{\partial F_{POP}}{\partial z}$, i.e. the divergence of the model's sinking flux of organic particulate phosphorus (F_{POP}), multiplied by a Redfield ratio for remineralization of -150. Note that this rate of respiration is converted to a concentration change by taking the time-integral over the length of the CO_2 -doubling simulation and subtracting the same quantity in the control simulation.

perturbed circulation slows the shoaling of the mixed layer would be shared among models or, more importantly, realized in nature. Given this uncertainty, we wish to emphasize the results that are more likely to be universal: i.e. that oxygenation of a large volume of the ocean depends on water mass formation processes in the Southern Ocean, and that oceanic deoxygenation is sensitive to changes in these processes. Indeed, 20th century deoxygenation has been observed to a depth of 3000 m in the Southern Ocean south of 50°S, contributing 15.8% of the total global deoxygenation, the second largest contribution of any ocean basin

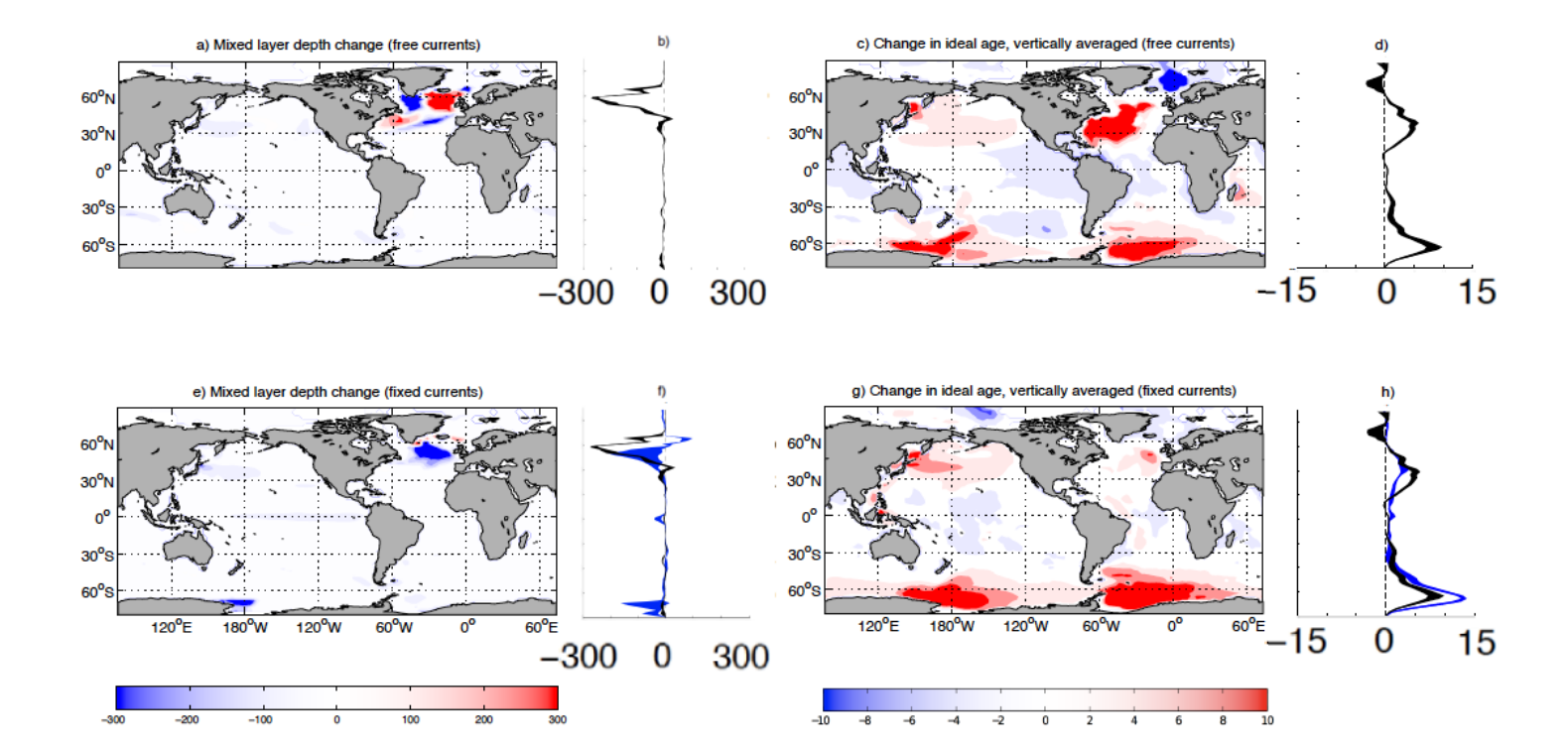


Figure 4. Maps of the change in mixed layer depth (left hand panels) and vertically averaged ideal age (right hand panels). The V_{free} simulation is shown in the top row and the V_{fixed} simulation in the bottom row. Line plots (b, d, f and h) give the zonal mean of the plot to their left. On the line plots in the bottom row the blue line is for the V_{fixed} simulation and black line reproduces the zonal mean of the V_{free} simulation for comparison. Note that the color scale for the left hand panels saturates below the maximum values to emphasize spatial patterns.

globally and slightly larger than the contribution of the Southern Ocean to total ocean volume [Schmidtko et al., 2017].

The ideal age tracer evolves differently outside the Southern Ocean. In the North Pacific, the change in ideal age is only subtly different between V_{free} and V_{fixed} , suggesting that the dominant control on water column aging in this region is due to the small decline in mixed layer depth (Figure 4, left-hand panels). We note that both our use of ensemble averages and focus on 20-year mean properties at the end of a period of strong radiative forcing suppress the influence of internal variability of North Pacific circulation, which has been shown to be a leading driver of interannual to decadal oxygen variability in previous studies [Deutsch et al., 2005, 2006; Mecking et al., 2008]. In contrast with the North Pacific and

Southern Ocean, the circulation perturbation in the North Atlantic causes a greater shoaling of the basin-average mixed layer depth and slows the delivery of newly-ventilated waters to the midlatitudes, thereby increasing the ideal age more strongly in V_{free} .

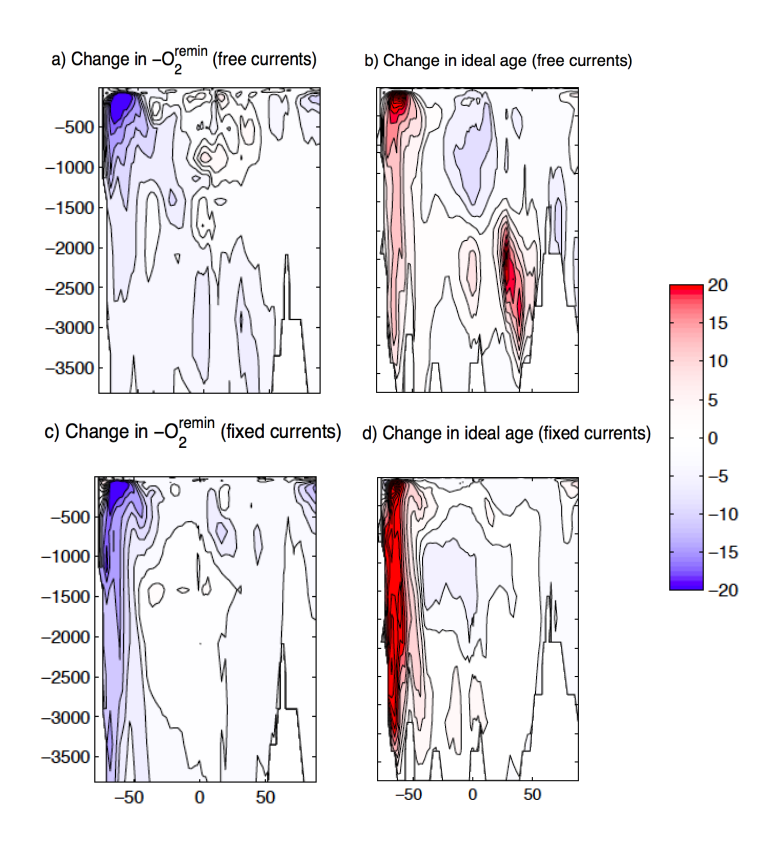


Figure 5. Zonally averaged O_2^{remin} (left hand panels) and ideal age (right hand panels) in the Atlantic Ocean, plotted as a function of depth and latitude. The V_{free} simulation is shown in the top row (a,b) and the V_{fixed} simulation in the bottom row (c,d). Again, O_2^{remin} has been multiplied by negative one so that negative values correspond with a decrease in total O_2 .

Schmidtko et al. [2017] recently conjectured that a slowdown in the AMOC would rapidly deplete the deep ocean oxygen reservoir by denying the advective transport of newly formed and well-oxygenated deep and bottom water. This effect is not evident in the vertically-integrated O_2 reservoir in the North Atlantic in our simulations, despite a 25% slowdown in the AMOC and an associated increase in ideal age in the deep North Atlantic below 2000 m, between $20\text{-}50^\circ\text{N}$ (Figure 5). This deep aging does not produce a large change in O_2^{remin} over the 70-year simulation, because it is at a depth where the sinking flux of organic matter is small and respiration relatively slow. Notably, both ideal age and O_2^{remin} increase much more rapidly at shallower layers in the Southern Ocean than the North Atlantic.

3.2 The stabilizing effect of ocean circulation on oxygen concentrations in the Pacific OMZ

Of particular consequence in the discussion of ocean deoxygenation is the expansion and/or intensification of the Pacific Oxygen Minimum Zone (OMZ), the largest OMZ in the world ocean. The Pacific OMZ has lost oxygen during the observational era [Schmidtko et al., 2017], but model simulations under climate change produce only slow rates of change in this region, and are not consistent even on the sign of these trends [Cabré et al., 2015]. CMIP5 models show very low rates of change in Pacific OMZ because of competing trends in O_2^{sat} and AOU [Cabré et al., 2015], both of which decline (at these low latitudes, ΔO_2^{sat} is a good proxy for ΔO_2^{pref} - see Figure 2). Similar to the average of the CMIP5 suite, our V_{free} simulation has very little change in O_2 concentration at the depth of the oxygen minimum in the eastern tropical Pacific (Figure 6). This result also holds when analyzing at fixed

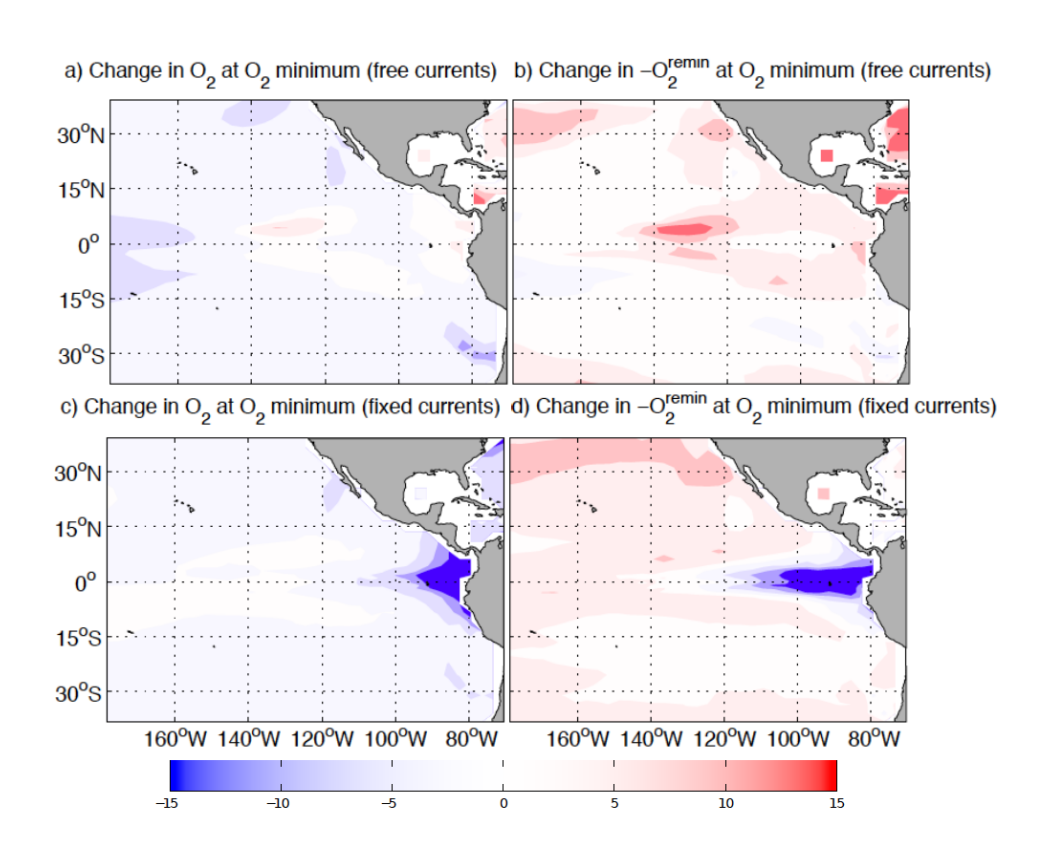


Figure 6. Ensemble mean O_2 concentrations (mmol m⁻³) at the O_2 minimum in the Eastern Tropical Pacific. V_{free} is in the top row (a, b) and V_{fixed} in the bottom row (c, d). Total O_2 concentrations are on the left (a, c); O_2^{remin} is on the right (b, d). Again, O_2^{remin} has been multiplied by negative one so that negative values correspond with a decrease in total O_2 .

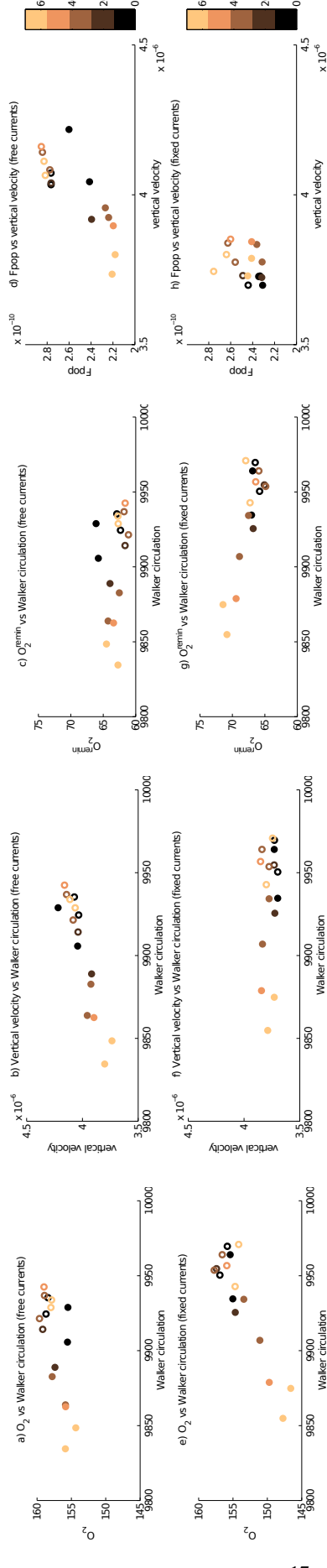


Figure 7. Scatterplot time series exploring the role of the Walker Circulation and upwelling on O₂ concentrations and export productivity in the Eastern Tropical Pacific. Open dots 5°N minus 100-160°E, 5°S-5°N. a,e) O₂ concentrations (mmol m⁻³) versus Walker Circulation strength (Pa); b,f) Upwelling velocity (m s⁻¹) versus Walker Circulation strength; c,g) Vfixed. All oceanic averages are taken over the box 80-115°W, 10°S-10°N. The Walker Circulation is calculated as the difference in sea level pressure averaged over 80-160°W, 5°Sare for the control simulation and filled dots for the CO₂ doubling simulation. The color of the dots shows the year (1-70) of the simulation. Top row is for V_{free} and bottom row for O_{c}^{emin} versus Walker Circulation strength; d,h) Export production (mol m⁻² s⁻¹) versus upwelling velocity (m s⁻¹).

depths. In contrast, the V_{fixed} simulation realizes a precipitous drop of 15 mmol m⁻³ in the Pacific OMZ as CO₂ doubles, largely due to an increase in O_2^{remin} . Thus, the comparison of V_{free} to V_{fixed} implies that the ocean circulation perturbation is a stabilizing force on O_2^{remin} in the Pacific OMZ, thereby preventing the intensification of the oxygen minimum.

To look more closely at the mechanisms preventing O_2 decline in the Pacific OMZ, we compare time series of the relationship between various properties in this region (Figure 7). Here, previous work has suggested that the tropical atmospheric circulation cell, called the Walker Circulation, which sets the strength of the equatorial wind stress, may strongly influence O_2 respiration via its influence on the upwelling of nutrients and resultant export productivity [*Deutsch et al.*, 2014]. A predicted weakening of the Walker Circulation is shared among many, but not all, climate models, a trend that is additionally hard to distinguish from large interannual to multidecadal flucations [*Plesca et al.*, 2017]. A slowdown of the Walker Circulation is predicted by the ensemble mean of both V_{free} and V_{fixed} , with the ensemble-averaging helping to distinguish the trend from variability. In our model, the Walker Circulation values for the CO_2 doubling ensemble means are clearly outside the range of variability in the control simulations (Figure 7). This slowdown weakens the easterly trade winds over the tropical Pacific (Figure 7a/e) in both V_{fixed} and V_{free} . However, this weakening manifests as a drop in O_2 only in V_{fixed} (Figure 7a/e).

In the V_{free} simulation, the slackening of the winds reduces upwelling (Figure 7b), an effect that is suppressed in V_{fixed} (Figure 7f). In turn, the reduced upwelling in V_{free} slows the vertical supply of nutrients to the euphotic zone, weakening primary productivity and the export of organic matter past the base of the shallow mixed layer (Figure 7d). With reduced substrate for respiration, the consumption of O_2 slows, as reflected in O_2^{remin} (Figure 7c) being stable over the length of the V_{free} simulation. In contrast, in V_{fixed} , the influence of the Walker slowdown manifests solely in subgridscale processes in the ocean, mainly through a reduction in wind-driven mixing. The resulting shoaling of the mixed layer depth (Figure 4) and decrease in ventilation leads to an increase in O_2^{remin} (Figures 6 and 7g). Thus, the comparison of the simulation reveals that the perturbation to upwelling linked to the Walker slowdown slows the pace of hypoxic intensification. This mechanism for governing the size of Pacific OMZ agrees with that proposed by $Deutsch\ et\ al.\ [2014]$ based on a centennial scale reconstruction of sea level pressure and nitrogen isotopes in the region.

4 Conclusions

Our simulations reveal that the rate and spatial patterns of ocean deoxygenation are, to first order, set by changes in mixing and solubility. However, the adjustment of the large-scale circulation can alter these changes. In our simulations, the adjustment of the large-scale ocean circulation under a doubling of atmospheric CO₂ helps to maintain deeper mixed layers in Southern Ocean regions of dense water formation. Thus, the residence time of the deep ocean increases more slowly. Though we caution that this feedback between ocean circulation and Antarctic mixed layer depths may be a model-dependent response, it underscores the sensitivity of the global oxygen reservoir to small changes in deep water formation regions, particularly in the Southern Ocean. In addition to these changes in residence time, global average export productivity and associated respiration also declines, a common result in climate models responding to radiative forcing [Sarmiento et al., 2004; Bopp et al., 2002]. With both respiration rates slower and the residence time of the water in the ocean interior somewhat stabilized, global average ocean deoxygenation is reduced relative to the idealized simulation in which the ocean circulation is held steady despite a changing climate.

Another notable result is that globally-averaged preformed oxygen concentrations changes are smaller than would be inferred from the change in solubility due to warming. The change in O_2^{sat} is a poor proxy of the change in O_2^{pref} at high latitudes, because the warming is accompanied by a slowdown in the rate at which of O_2 -depleted water comes to the surface and is subsequently subducted into the ocean interior still undersaturated in oxygen. This effect is related to the disequilibrium pump of carbon discussed by *Ito and Follows* [2013], whereby the the excess carbon upwelled to the surface of the Southern Ocean is not degassed to the atmosphere but re-enters into the deep ocean due to the incomplete air-sea equilibration. However, the effect is smaller for O_2 , because it equilibrates more quickly than CO_2 . And, while the disequilibrium pump allows for the ocean to store more carbon relative to the situation of instantaneous equilibration, it results in a smaller oxygen reservoir. This result should alert the community to use caution when interpreting the change in O_2^{sat} as the contribution of warming to deoxygenation, as it can lead to overestimates of the solubility effect by about 10% in the global averaged, with greater errors at high latitudes.

Finally, in our simulations, the Walker simulation declines under a doubling of CO₂, due to changes in zonal temperature gradients [*Trossman et al.*, 2016], which prevents the expansion and intensification of the Pacific OMZ. A caveat on this point is that the Walker

Circulation has substantial temporal variability, and its slowdown is not a universal response to warming in models [*Plesca et al.*, 2017]. As proposed in previous papers [*Deutsch et al.*, 2014; *Cabré et al.*, 2015], when the upwelling of nutrients in the tropical Pacific slows under the weaker Walker Circulation, there is lower export production, respiration of exported organic matter, and a stabilization of Pacific OMZ. Thus, on both global and on some regional scales, the ocean circulation perturbation can work towards slowing the decline in oceanic O₂ concentrations.

It is important to note that a decline in primary productivity contributes a small slow-down in the amount of substrate available for respiration globally. However, as globally averaged oxygen utilization rates decrease slightly, this decrease is overwhelmed by a more rapid decrease in mixing and advection of O_2 into the ocean interior, collectively referred to as ventilation. The AMOC slowdown, previously hypothesized to lead to deep deoxygenation by slowing the supply of newly ventilated water masses, had a small net impact on deep oxygen concentrations in the deep North Atlantic, over our 70 year simulations. Though the deep North Atlantic sees an increased residence time due to AMOC slowdown, it does not translate to a substantial deep O_2 decline because of slow respiration rates in these deep layers.

Acknowledgments

Acknowledgements: The authors gratefully acknowledge two reviewers whose insightful comments helped to improve an earlier version of this manuscript. We also thank Michael Havas for computer support, Eric Galbraith for his help with CM2Mc, and SciNet of Compute Canada for the computing resources. Funding from from Canada's NSERC Discovery Program, Québec's FRQNT, McGill University, and the University of Rhode Island made this research possible. Model output generated for this study is available upon request.

References

Bernardello, R., I. Marinov, J. B. Palter, J. L. Sarmiento, E. D. Galbraith, and R. D. Slater

(2014), Response of the Ocean Natural Carbon Storage to Projected Twenty-First-Century

Climate Change, *Journal of Climate*, 27(5), 2033–2053, doi:10.1175/JCLI-D-13-00343.1.

Bianchi, D., J. P. Dunne, J. L. Sarmiento, and E. D. Galbraith (2012), Data-based estimates

of suboxia, denitrification, and N2O production in the ocean and their sensitivities to dis
solved O2, *Global Biogeochemical Cycles*, 26(2), n/a–n/a, doi:10.1029/2011GB004209.

- Bopp, L., C. Le Quéré, M. Heimann, A. C. Manning, and P. Monfray (2002), Climate-
- induced oceanic oxygen fluxes: Implications for the contemporary carbon budget, Global
- Biogeochemical Cycles, 16(2), 6–1, doi:10.1029/2001GB001445.
- Bryan, F. O., P. R. Gent, and R. Tomas (2014), Can Southern Ocean Eddy Effects Be Param-
- eterized in Climate Models?, *Journal of Climate*, 27(1), 411–425, doi:10.1175/JCLI-D-
- 12-00759.1.
- ⁴⁷³ Cabré, A., I. Marinov, and S. Leung (2014), Consistent global responses of marine ecosys-
- tems to future climate change across the IPCC AR5 earth system models, *Climate Dynam-*
- *ics*, doi:10.1007/s00382-014-2374-3.
- Cabré, A., I. Marinov, R. Bernardello, and D. Bianchi (2015), Oxygen minimum zones in the
- tropical Pacific across CMIP5 models: mean state differences and climate change trends,
- Biogeosciences Discussions, 12(8), 6525–6587, doi:10.5194/bgd-12-6525-2015.
- Ciais, P., C. Sabine, G. Bala, L. Bopp, V. Brovkin, J. Canadell, A. Chhabra, R. DeFries,
- J. Galloway, M. Heimann, C. Jones, C. Le Quéré, R. Myneni, S. Piao, and P. Thornton
- (2013), Carbon and Other Biogeochemical Cycles. In: Climate Change 2013: The Physi-
- 482 cal Science Basis. Contribution of Working Group I to the Fifth Assessment Report of the
- Intergovernmental Panel on Climate Change, chap. 6, Cambridge University Press, Cam-
- bridge, United Kingdom and New York, NY, USA.
- Deutsch, C., S. Emerson, and L. Thompson (2005), Fingerprints of climate change
- in North Pacific oxygen, *Geophysical Research Letters*, 32(16), L16,604, doi:
- 10.1029/2005GL023190.
- Deutsch, C., S. Emerson, and L. Thompson (2006), Physical-biological interactions in North
- 489 Pacific oxygen variability, J. Geophys. Res., 111(C9), C09S90, doi:10.1029/2005jc003179.
- Deutsch, C., W. Berelson, R. Thunell, T. Weber, C. Tems, J. McManus, J. Crusius, T. Ito,
- T. Baumgartner, V. Ferreira, J. Mey, and A. van Geen (2014), Oceanography. Centennial
- changes in North Pacific anoxia linked to tropical trade winds., Science (New York, N.Y.),
- 493 345(6197), 665–8, doi:10.1126/science.1252332.
- Deutsch, C., A. Ferrel, B. Seibel, H.-O. Portner, and R. B. Huey (2015), Climate change
- tightens a metabolic constraint on marine habitats, Science, 348(6239), 1132–1135, doi:
- 496 10.1126/science.aaa1605.
- Dunne, J. P., J. G. John, A. J. Adcroft, S. M. Griffies, R. W. Hallberg, E. Shevliakova, R. J.
- Stouffer, W. Cooke, K. A. Dunne, M. J. Harrison, J. P. Krasting, S. L. Malyshev, P. C. D.
- Milly, P. J. Phillipps, L. A. Sentman, B. L. Samuels, M. J. Spelman, M. Winton, A. T. Wit-

- tenberg, and N. Zadeh (2012), GFDL's ESM2 global coupled climate-carbon Earth System
- Models Part I: Physical formulation and baseline simulation characteristics, *Journal of*
- 502 *Climate*, doi:10.1175/jcli-d-11-00560.1.
- Duteil, O., W. Koeve, A. Oschlies, D. Bianchi, E. Galbraith, I. Kriest, and R. Matear (2013),
- A novel estimate of ocean oxygen utilisation points to a reduced rate of respiration in the
- ocean interior, *Biogeosciences*, 10(11), 7723–7738, doi:10.5194/bg-10-7723-2013.
- Galbraith, E. D., E. Y. Kwon, A. Gnanadesikan, K. B. Rodgers, S. M. Griffies, D. Bianchi,
- J. L. Sarmiento, J. P. Dunne, J. Simeon, R. D. Slater, A. T. Wittenberg, and I. M. Held
- 508 (2011), Climate Variability and Radiocarbon in the CM2Mc Earth System Model, *Journal*
- of Climate, 24(16), 4230–4254, doi:10.1175/2011jcli3919.1.
- Galbraith, E. D., J. P. Dunne, A. Gnanadesikan, R. D. Slater, J. L. Sarmiento, C. O. Dufour,
- G. F. de Souza, D. Bianchi, M. Claret, K. B. Rodgers, and S. S. Marvasti (2015), Complex
- functionality with minimal computation: Promise and pitfalls of reduced-tracer ocean bio-
- geochemistry models, Journal of Advances in Modeling Earth Systems, 7(4), 2012–2028,
- doi:10.1002/2015MS000463.
- Gent, P. R., and J. C. McWilliams (1990), Isopycnal mixing in ocean circulation models,
- Journal of Physical Oceanography, 20, 150–155.
- Gnanadesikan, A., and I. Marinov (2008), Export is not enough: nutrient cycling and carbon
- sequestration, Marine Ecology Progress Series, 364, 289–294, doi:10.3354/meps07550.
- Griffies, S. M., A. Gnanadesikan, K. W. Dixon, J. P. Dunne, R. Gerdes, M. J. Harrison,
- A. Rosati, J. L. Russell, B. L. Samuels, M. J. Spelman, M. Winton, and R. Zhang (2005),
- Formulation of an ocean model for global climate simulations, *Ocean Science*, 1(1), 45–
- 522 79.
- Griffies, S. M., M. Winton, W. G. Anderson, R. Benson, T. L. Delworth, C. O. Dufour, J. P.
- Dunne, P. Goddard, A. K. Morrison, A. Rosati, A. T. Wittenberg, J. Yin, R. Zhang, S. M.
- Griffies, M. Winton, W. G. Anderson, R. Benson, T. L. Delworth, C. O. Dufour, J. P.
- Dunne, P. Goddard, A. K. Morrison, A. Rosati, A. T. Wittenberg, J. Yin, and R. Zhang
- 527 (2015), Impacts on Ocean Heat from Transient Mesoscale Eddies in a Hierarchy of Cli-
- mate Models, *Journal of Climate*, 28(3), 952–977, doi:10.1175/JCLI-D-14-00353.1.
- Ito, T., and M. J. Follows (2013), Air-sea disequilibrium of carbon dioxide enhances the bio-
- logical carbon sequestration in the Southern Ocean, Global Biogeochemical Cycles, 27(4),
- 1129–1138, doi:10.1002/2013GB004682.

- Ito, T., M. J. Follows, and E. A. Boyle (2004), Is AOU a good measure of respiration in the oceans?, *Geophysical Research Letters*, *31*(17), n/a–n/a, doi:10.1029/2004GL020900.
- Ito, T., S. Minobe, M. C. Long, and C. Deutsch (2017), Upper ocean O2 trends: 1958-2015, *Geophysical Research Letters*, doi:10.1002/2017GL073613.
- Kelly, K. A. (2004), The relationship between oceanic heat transport and surface fluxes in the Western North Pacific: 1970-2000, *Journal of Climate*, *17*(3), 573–588, doi:
- 10.1175/1520-0442(2004)017<0573:TRBOHT>2.0.CO;2.
- Matear, R. J., and A. C. Hirst (2003), Long-term changes in dissolved oxygen concentrations in the ocean caused by protracted global warming, *Global Biogeochemical Cycles*, *17*(4),
- n/a–n/a, doi:10.1029/2002GB001997.
- Mecking, S., C. Langdon, R. A. Feely, C. L. Sabine, C. A. Deutsch, and D.-H. Min (2008),
- Climate variability in the North Pacific thermocline diagnosed from oxygen measure-
- ments: An update based on the U.S. CLIVAR/CO ₂ Repeat Hydrography
- cruises, Global Biogeochemical Cycles, 22(3), n/a–n/a, doi:10.1029/2007GB003101.
- Milly, P. C. D., and A. B. Shmakin (2002), Global Modeling of Land Water and Energy Bal-
- ances. Part I: The Land Dynamics (LaD) Model, *Journal of Hydrometeorology*, 3(3), 283–
- 299, doi:10.1175/1525-7541(2002)003<0283:GMOLWA>2.0.CO;2.
- O'Reilly, C. H., M. Huber, T. Woollings, and L. Zanna (2016), The signature of low-
- frequency oceanic forcing in the Atlantic Multidecadal Oscillation, *Geophysical Research*
- Letters, 43(6), 2810–2818, doi:10.1002/2016GL067925.
- Plesca, E., V. Grützun, S. A. Buehler, E. Plesca, V. Grützun, and S. A. Buehler (2017), How robust is the weakening of the Pacific Walker circulation in CMIP5 idealized transient cli-
- mate simulations?, *Journal of Climate*, pp. 17–0151, doi:10.1175/JCLI-D-17-0151.1.
- Rose, B. E. J., K. C. Armour, D. S. Battisti, N. Feldl, and D. D. B. Koll (2013), The depen-
- dence of transient climate sensitivity and radiative feedbacks on the spatial pattern of
- ocean heat uptake.
- Rugenstein, M. A. A., M. Winton, R. J. Stouffer, S. M. Griffies, and R. Hallberg (2012),
- Northern High-Latitude Heat Budget Decomposition and Transient Warming, *Journal*
- of Climate, 26(2), 609–621, doi:10.1175/jcli-d-11-00695.1.
- Rugenstein, M. A. A., K. Caldeira, and R. Knutti (2016), Dependence of global radiative
- feedbacks on evolving patterns of surface heat fluxes, Geophysical Research Letters, doi:
- 563 10.1002/2016GL070907.

- Sarmiento, J. L., T. M. C. Hughes, R. J. Stouffer, and S. Manabe (1998), Simulated response
- of the ocean carbon cycle to anthropogenic climate warming, *Nature*, *393*, 245–249.
- Sarmiento, J. L., R. Slater, R. Barber, L. Bopp, S. C. Doney, A. C. Hirst, J. Kleypas,
- R. Matear, U. Mikolajewicz, P. Monfray, V. Soldatov, S. A. Spall, and R. Stouffer (2004),
- Response of ocean ecosystems to climate warming, Global Biogeochemical Cycles, 18(3).
- 569 Schmidtko, S., L. Stramma, and M. Visbeck (2017), Decline in global oceanic oxygen con-
- tent during the past five decades, *Nature*, 542(7641), 335–339, doi:10.1038/nature21399.
- 571 Stramma, L., G. C. Johnson, J. Sprintall, and V. Mohrholz (2008), Expanding Oxygen-
- Minimum Zones in the Tropical Oceans, *Science*, 320(5876), 655–658, doi:
- 573 10.1126/science.1153847.
- 574 Stramma, L., E. D. Prince, S. Schmidtko, J. Luo, J. P. Hoolihan, M. Visbeck, D. W. R. Wal-
- lace, P. Brandt, and A. Körtzinger (2011), Expansion of oxygen minimum zones may re-
- duce available habitat for tropical pelagic fishes, *Nature Climate Change*, 2(1), 33–37,
- doi:10.1038/nclimate1304.
- Trossman, D. S., J. B. Palter, T. M. Merlis, Y. Huang, and Y. Xia (2016), Large-scale ocean
- circulation-cloud interactions reduce the pace of transient climate change, Geophysical
- Research Letters, 43(8), 3935–3943, doi:10.1002/2016GL067931.
- Winton, M. (2003), On the Climatic Impact of Ocean Circulation, *Journal of Climate*,
- 582 16(17), 2875–2889, doi:10.1175/1520-0442(2003)016<2875:OTCIOO>2.0.CO;2.
- Winton, M., S. M. Griffies, B. L. Samuels, J. L. Sarmiento, and T. L. Frölicher (2013), Con-
- necting Changing Ocean Circulation with Changing Climate, *Journal of Climate*, 26(7),
- ⁵⁸⁵ 2268–2278, doi:10.1175/JCLI-D-12-00296.1.